Electronic and optical properties of RuO_2 and IrO_2

J. S. de Almeida* and R. Ahuja
Condensed Matter Theory Group, Department of Physics, Uppsala University, Box 530, S-751 21 Uppsala, Sweden
(Received 22 June 2005; revised manuscript received 21 November 2005; published 4 April 2006)

We report first principles self-consistent electronic structure calculations of RuO_2 and IrO_2 using the full-potential linearized augmented plane wave method. Our electronic properties are in good agreement with x-ray photoelectron spectroscopy data regarding the bandwidths and peak positions. Additionally, we probe our electronic structures by calculating the dielectric functions and comparing them with optical measurements. Our calculations show that intraband transitions play an important role to describe properly the optical response of RuO_2 and IrO_2. We find that these materials are good absorbers at low energies where the dielectric functions exhibit a Drude like behavior. At higher energies, the optical features are due to electronic transitions from oxygen $2p$ to metal d bands. Our results for the dielectric functions and energy loss spectra show a good agreement with optical measurements.

DOI: 10.1103/PhysRevB.73.165102 PACS number(s): 71.15.Mb, 71.20.−b, 78.20.Bh

I. INTRODUCTION

The transition metal dioxide (MO_2) compounds are interesting from fundamental and technological points of view. For example, the electrical conductivity changes in several orders of magnitude in this class of materials. There are also paramagnetic, ferromagnetic, and antiferromagnetic compounds among them where one can study a wide range of physical phenomena.[1] On the other hand, research of oxide materials have increased over the last decade, especially driven by the technological requirements for microwave communication systems, infrared imaging systems, highly sensitive detectors, and also by the search of materials for improved ferroelectric memories, optical devices, and magnetic sensors.

In particular, ruthenium dioxide (RuO_2) has low resistance, high thermal, and chemical stabilities at ambient conditions yielding a good material for applications such as corrosion-resistant low overpotential electrodes for chlorine or oxygen evolution and a catalytic agent for photodissociation of water.[2,3] Moreover, it is a promising material for use as a strip-line conductor in integrated circuits and also for electrical contacts.[4,5] Iridium dioxide (IrO_2), on the other hand, can be used as electrode material for production of components in advanced memory technologies. Igarashi *et al.*[6] produced submicrometer ferroelectric capacitors for high-density ferroelectric memories and IrO_2-based resistors were prepared for application in piesoresistive sensors.[7] Due to its color change by applying a small voltage or current, a remarkably fast response to anodic coloration and cathodic bleaching, IrO_2 is a promising electrochromic material.[8]

Besides their great importance information is still needed about the electronic and optical properties of these materials. The first theoretical investigation of the electronic structure of RuO_2 and IrO_2 was done by Mattheiss in a non-self-consistent calculation using the linear combination of atomic orbitals method to fit augmented-plane wave (APW-LCAO) results.[9] These calculations reproduce qualitatively well the electronic bands of RuO_2 and IrO_2 but do not describe correctly the width of the bands and give a large energy gap between oxygen $2p$ and metal d states. Indeed, a large p-d gap yields an overestimation of the covalent character between these bands. By measuring the reflectivity of RuO_2 and IrO_2, Goel *et al.*[10] suggested that the p-d energy gap is about 1 eV smaller than the theoretical APW-LCAO results. Xu *et al.*[11] studied the electronic and optical properties of these materials using self-consistent calculations based on the linear muffin tin orbitals (LMTO) method and atomic sphere approximation (ASA). As one might expect, they found that self-consistency is important in positioning the oxygen $2p$ bands below the Fermi level because of the charge transfer in metallic oxides.

Subsequently, a major number of theoretical investigations has been carried out for RuO_2 compared to IrO_2. Electronic and optical properties of RuO_2 were performed using *ab initio* theory.[12–15] However, in all these calculations a certain approximation of the actual crystalline potential was used and this could affect the width of the bands and the peak binding energies. The only full-potential calculation of the electronic properties of RuO_2 was reported by Sorantin and Schwarz.[16] Since RuO_2 is a metal, it was claimed[14] that the accuracy of their results could be affected by the convergence criteria (e.g., small number of **k**-points) used in the calculation. In the case of IrO_2, to the best of our knowledge, there is no report on the electronic structure using full potential based methods and a theoretical investigation of the dielectric function does not even exist.

In this paper we investigate electronic and optical properties of RuO_2 and IrO_2 as well as the issue on the degree of covalency between oxygen and metal atoms. In order to avoid possible errors arising from the crystalline potential which could affect the binding energies, the width of the bands and the optical response of these materials we have used a very accurate state-of-the-art all electron method. Self-consistent electronic structure calculations were performed without using any geometrical approximation of the crystalline potential while the optical properties were studied by means of the dielectric function and energy loss spectrum. In our calculations, the dielectric functions were evaluated taking into account interband and intraband electronic transitions.

The paper is organized as follows: in Sec. II we describe the computational details, Sec. III we discuss the results for electronic structure of RuO_2 and IrO_2 whereas the optical properties are presented in the Sec. IV. Finally, we summarize our findings in Sec. V.

II. COMPUTATIONAL METHODS

The electronic properties of RuO_2 and IrO_2 were theoretically studied by means of first principles calculations in the framework of density functional theory (DFT) and based on the full-potential linearized augmented plane wave (FP-LAPW) method as implemented in the WIEN2K code.[17] The core states were treated fully relativistically[18] while for valence states the scalar relativistic treatment[19] without spin-orbit coupling was employed. We have used the generalized gradient approximation (GGA) for the exchange and correlation potential.[20] The muffin tin radius (R_{mt}) of the atomic spheres was chosen to be 1.8 a.u. for Ru, 1.8 a.u. for Ir, and 1.7 a.u. for O. The number of plane waves is determined by the product $R_{mt}K_{max}$, where K_{max} is the largest reciprocal vector used in the LAPW basis set. In our calculations, we set $R_{mt}K_{max}=9$ which gives about 1500 plane waves to describe valence and semicore states. The charge density and potentials were expanded up to $l=10$ inside the atomic spheres, and the total energies difference were converged to below 10^{-4} eV with respect to Brillouin zone integration. For the sampling of the Brillouin zone we made use of a $12\times12\times18$ shifted **k**-point grid generated according to the Monkhorst-Pack scheme.[21]

III. ELECTRONIC PROPERTIES

These compounds crystallize in the rutile phase and have a tetragonal structure containing two MO_2 formula units per cell with atoms M located at (0,0,0) and (0.5,0.5,0.5) positions and atoms O positioned at $\pm(u,u,0)$ and $\pm(0.5+u,0.5-u,0.5)$, where u is the internal parameter. The crystal structure belongs to the space group $P4_2/mnm$. The calculations were done assuming the experimental lattice constants with values of $a=8.488$ a.u., $c=6.048$ a.u., and $u=0.306$ for RuO_2 and $a=8.500$ a.u., $c=5.961$ a.u., and $u=0.307$ for IrO_2.[22,23]

In Figs. 1 and 2, we plot the electronic band structures along the high symmetry points in the Brillouin zone (BZ) together with the density of states (DOS) for RuO_2 and IrO_2, respectively. The Fermi level (E_F) is set as zero of energy and indicated by a horizontal dashed line.

From Fig. 1, we see the following set of bands: four oxygen 2s, twelve oxygen 2p, and ten ruthenium 4d bands. The lower valence band formed by O 2s states is about 20.2 eV below the Fermi level with a bandwidth (W) of 2 eV and the peak position at −18.6 eV. The width of O 2s bands is 0.7 eV smaller than the pseudopotential[12] result but it is close to the value found by Sorantin and Schwarz.[16] The binding energy of the O 2s bands is consistent with most of the *ab initio* calculations[12–16] but it is usually underestimated by approximately 3 eV when compared to experimental results.[24,25] This disagreement is probably due to the difficulty of the theory to describe semicorelike states, the experimental resolution, and electronic relaxation effects, where the latter is typically around 1 eV as pointed out by Glassford and Chelikowsky.[12]

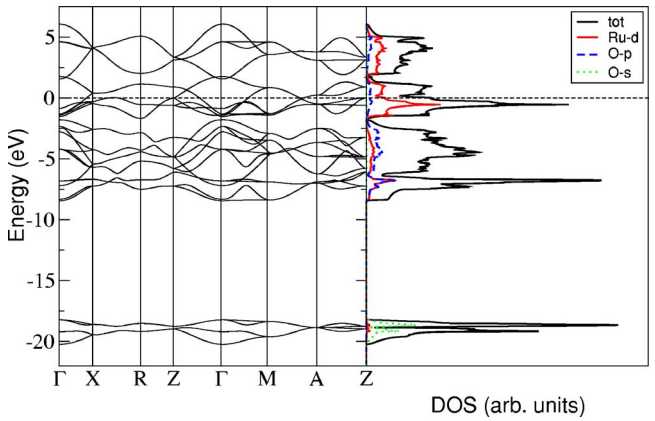

FIG. 1. (Color online) Energy band structure (left panel) along the high symmetry points in the Brillouin zone and density of states (right panel) for RuO_2. Partial DOS: Ru 4d (full line) states, O 2p (dashed line) states, and O 2s (dotted line) states. The Fermi level is set as zero energy and indicated by a horizontal dashed line.

As shown in Fig. 1, the upmost valence bands arise from the ruthenium-oxygen σ- and π-bonding orbitals. This band with predominant O 2p character is formed at −8.5 eV having a bandwidth of 6.7 eV while x-ray photoelectron spectroscopy (XPS) measurements[24,25] show a bandwidth of nearly 7 eV and the edge located at around −9 eV. Krasovska *et al.*[14] found 5.9 eV bandwidth for the O 2p manifold and they claimed that their result is in better agreement with XPS data[25] then 6.5 eV according to Sorantin and Schwarz.[16] They argued that the difference between the two results is probably due to the small number of **k** points which causes interpolation errors in the integration over the Brillouin zone. Although we use a very large number of **k** points in our calculations, we find that the width of O 2p manifold is almost the same ($W=6.5$ eV) as reported by Sorantin and

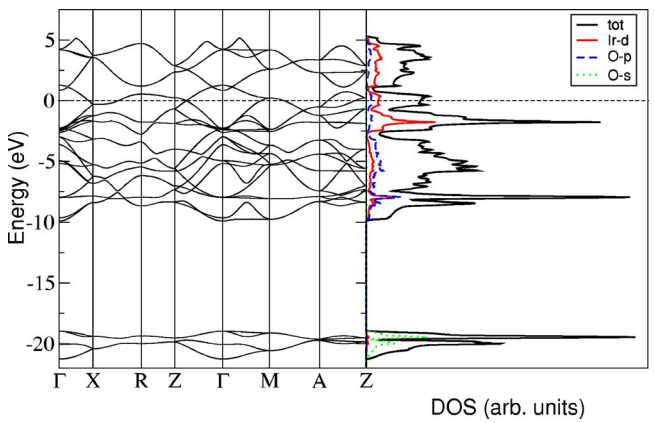

FIG. 2. (Color online) Energy band structure (left panel) along the high symmetry points in the Brillouin zone and density of states (right panel) for IrO_2. Partial DOS: Ir 5d (full line) states, O 2p (dashed line) states, and O 2s (dotted line) states. The Fermi level is set as zero energy and indicated by a horizontal dashed line.

Schwarz.[16] We attribute such a difference to the crystalline potential because of the muffin-fin tin approximation used in the calculation by Krasovska *et al.* A bandwidth of nearly 7 eV for the O $2p$ manifold has also been confirmed by other self-consistent calculations[11,12,15] and a slight deviation of this value is expected. Moreover, a precise comparison is likely difficult because of the broadening of the spectra and the experimental resolution.

The conduction band (Fig. 1) is composed mainly by Ru $4d$ states which are split into a set of partially occupied t_{2g} and unoccupied e_g bands having a width of 3.4 and 4.3 eV, respectively. The Fermi level indicated by a horizontal dashed line is near the minimum of the Ru t_{2g} manifold. From our DOS, we find that the occupation at the Fermi level is 1.97 states eV^{-1} $cell^{-1}$ $spin^{-1}$, which is close to the experimental value of 2.1 reported by Cox *et al.*[26] The low DOS at the Fermi level is responsible for the stabilization of the rutile phase of RuO_2 in contrast to tetragonal VO_2, where the Fermi level falls in a sharp peak of the t_{2g} bands leading to a structural phase transformation induced by temperature to a monoclinic phase.[16] As seen in Fig. 1, the peak of the Ru t_{2g} bands at 0.6 eV below the Fermi level arises mainly from the almost dispersionless bands along the R-Z, Z-Γ, and A-Z directions in the Brillouin zone. According to XPS data,[24,25] the binding energy of Ru t_{2g} bands is 0.6–0.8 eV which is in good agreement with our results as well as 0.7 and 0.68 eV reported in previous *ab initio* calculations.[12,14]

The O $2p$ and Ru $4d$ bands are well separated throughout the Brillouin zone with the smallest energy gap of 0.3 eV at the Γ point. Earlier, an empirical reduction of this p-d gap was suggested to understand the optical features in reflectivity measurements[10] based on the band structure results of Mattheiss.[9] Recently, the p-d gap has been reported in self-consistent calculations[11–16] from 0 to 0.4 eV rather than 1.5 eV found in the APW-LCAO calculations. Therefore, our results confirm the overestimated covalent character of these bands in the calculation by Mattheiss.

In Fig. 2, we identify the same set of electronic bands for IrO_2 as for RuO_2; the lower valence band is due to O $2s$ states, the upmost valence band is formed by hybridization between oxygen $2p$ and iridium $5d$ states whereas the conduction band is mostly Ir $5d$ states. Additionally, the shape of the band structure and DOS of the two compounds are similar but the Fermi level of IrO_2 is shifted upward because of the band filling effect and a larger c/a ratio. In this case, we find that the O $2s$ bands have a bandwidth of 2.3 eV with the peak located at 19.6 eV below the Fermi level whereas it is found at around −20.0 and −24.3 eV from APW-LCAO and LMTO-ASA calculations, respectively.[9,11] Experimentally, the peak of O $2s$ bands is observed at around 22 eV below the Fermi level.[25]

As illustrated in Fig. 2, we find that the upmost valence band with predominant O $2p$ character is formed at −10 eV and has a bandwidth of 7.5 eV. Previously, the width of this band has been reported as approximately 8 eV from XPS measurements,[25] 7.2 and 5.5 eV from LMTO-ASA and APW-LCAO calculations, respectively.[9,11] In contrast to RuO_2 results, we find that for IrO_2 the energy gap between O $2p$ and Ir $5d$ orbitals is reduced in the whole Brillouin zone which yields to a strong overlap of these orbitals and there is no tendency of gap formation between them at the Γ point. A reason for this is that Ir is heavier than Ru and its $5d$ electrons in the outer shell lead to a strong overlap with the O $2p$ electrons. The overestimated result of the bandgap between O $2p$ and Ir $5d$ states found by Mattheiss is 2 eV while the LMTO-ASA value is less than 0.5 eV. Since the shape of O $2p$ and Ir $5d$ bands are rather similar in the FP-LAPW and LMTO-ASA calculations, the difference of having no p-d bandgap in our result and the value found using LMTO-ASA is most probably due to inclusion of empty spheres and ASA in the latter calculation.

As seen in Fig. 2, the Ir $5d$ states are split into a set of partially occupied t_{2g} and unoccupied e_g bands having a bandwidth of 3.4 and 4.3 eV, respectively. As one can see, the peak of the Ir t_{2g} manifold at −1.8 eV is mostly due to flat double degenerated bands along the A-Z direction in the BZ. The binding energy of the Ir t_{2g} bands is about 1.8 eV according to XPS data[24,25] whereas it is 1.3 and 1.1 eV according to LMTO-ASA and APW-LCAO calculations. From our DOS, we find that the occupation at the Fermi level is 1.47 states eV^{-1} $cell^{-1}$ $spin^{-1}$ which is somewhat smaller than 2.02 and 2.09 states eV^{-1} $cell^{-1}$ $spin^{-1}$ reported by Mattheiss and Xu *et al.*, respectively.[9,11] However, it is clear from the DOS that a small shift in E_F might change the DOS(E_F) and this could explain the different occupations at the Fermi level.

IV. OPTICAL PROPERTIES

The optical properties are studied through the dielectric function as well as energy loss spectrum and the results are compared with experimental data taken from Ref. 10.

The optical response of crystals can be described by the complex dielectric function $\epsilon(\mathbf{q},\omega)$ where $\mathbf{q}$ is the momentum transfer in the electron-photon interaction and ω is the energy transfer. We have used the electric dipole approximation ($\mathbf{q}=0$) in this work.

The tetragonal symmetry of the crystal structures under consideration allow us to decompose the dielectric function $[\epsilon(\omega)=\epsilon_1(\omega)+i\epsilon_2(\omega)]$ into parallel ($\epsilon_\parallel$) and perpendicular ($\epsilon_\perp$) components.

The dielectric function of metallic like compounds such as RuO_2 and IrO_2 can be due to band to band (interband) electronic transitions and due to electronic transitions occurring within the same band (intraband). For the interband transitions, first we evaluate the imaginary part, $\epsilon_2(\omega)$, and thereafter we use the causality relation to calculate the real part. Hence, the imaginary part of the dielectric function[27] is calculated directly from the electronic structure through the joint density of states and the matrix elements of the momentum, $\mathbf{p}$, between occupied and unoccupied eigenstates

$$\epsilon_2^{ij}(\omega)=\frac{4\pi^2e^2}{\Omega m^2\omega^2}\sum_{\mathbf{k}nn'}\langle\mathbf{k}n|p_i|\mathbf{k}n'\rangle\langle\mathbf{k}n'|p_j|\mathbf{k}n\rangle \times f_{\mathbf{k}n}(1-f_{\mathbf{k}n'})\,\delta(E_{\mathbf{k}n'}-E_{\mathbf{k}n}-\hbar\omega). \quad (1)$$

In this equation, e is the electron charge, m its mass, Ω is the volume of crystal, $f_{\mathbf{kn}}$ is the Fermi distribution function

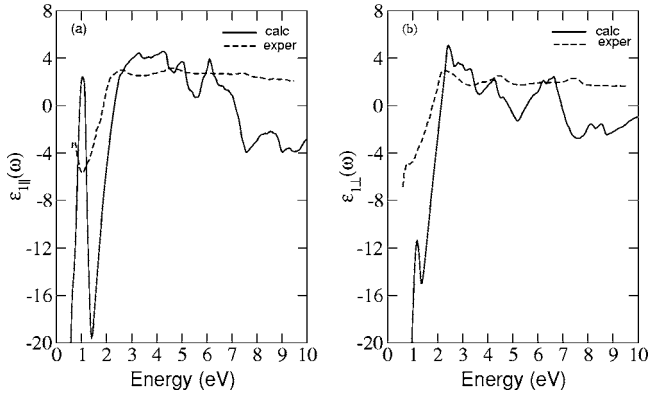

FIG. 3. Parallel (a) and perpendicular (b) components of the real part of the dielectric function versus photon energy for RuO_2.

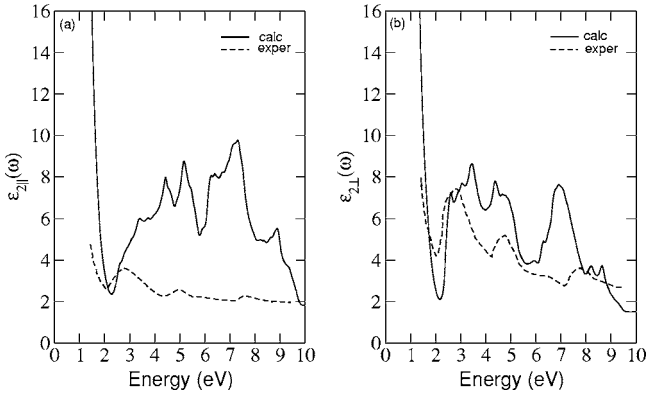

FIG. 4. Imaginary part of the dielectric function versus photon energy for RuO_2: parallel (a) and perpendicular (b) components.

and $|\mathbf{k}_n\rangle$ is the crystal wave function corresponding to the nth eigenvalue $E_{\mathbf{k}n}$ with the crystal wave vector $\mathbf{k}$. The integration in $\mathbf{k}$ space was done using the modified tetrahedron method with a grid containing about 4000 $\mathbf{k}$ points in the IBZ. The real part of the dielectric function is calculated via the Kramers-Kronig transformation

$$\epsilon_1(\omega) = 1 + \frac{1}{\pi}\int_0^\infty d\omega' \epsilon_2(\omega')\left(\frac{1}{\omega' - \omega} + \frac{1}{\omega' + \omega}\right). \quad (2)$$

For intraband transitions the imaginary and real parts of the dielectric function are

$$\epsilon_2^{ij}(\omega) = \frac{\gamma\omega_{p;ij}^2}{\omega(\omega^2 + \gamma^2)} \quad (3)$$

and

$$\epsilon_1^{ij}(\omega) = 1 - \frac{\omega_{p;ij}^2}{(\omega^2 + \gamma^2)}, \quad (4)$$

where γ is the lifetime broadening and $\omega_{p;ij}$ is the plasma frequency, which is given by

$$\omega_{p;ij}^2 = \frac{\hbar^2 e^2}{\pi m^2}\sum_{\mathbf{k}n} \langle \mathbf{k}n|p_i|\mathbf{k}n\rangle\langle \mathbf{k}n|p_j|\mathbf{k}n\rangle \delta(E_{\mathbf{k}n} - E_F) \quad (5)$$

with E_F being the Fermi energy.

The parallel and perpendicular components of real and imaginary parts of the dielectric function for RuO_2 are compared with experimental data in Figs. 3(a), 3(b), 4(a), and 4(b), respectively. From these figures, we see that our calculations reproduce qualitatively well the features observed in the experiment. However, the perpendicular components have a somewhat better agreement than the parallel ones.

In the parallel component of the ϵ_1 spectrum shown in Fig. 3(a), the optical structures are systematically shifted upwards by about 0.5 eV compared to the experimentally observed ones. For the parallel and perpendicular components of ϵ_1 spectra [Fig. 3], at energy of about 1 eV, both theoretical and experimental ϵ_1 spectra show a pronounced anisotropy that are assigned due to free electron excitations and interband transitions within Ru 4d bands. As seen in Fig. 4, the ϵ_2 spectra have a high absorption below 2 eV which is due to transitions within Ru t_{2g} bands while the other optical structures above 2 eV arise from $p \rightarrow d$ electronic transitions. The calculated and experimental absorption have a minimum around 2.5 eV which is the onset of the interband transitions where the Drude-like contributions fall off and the interband transitions take over. Additionally, the calculated parallel component of ϵ_2 spectrum [Fig. 4(a)] shows a broad shoulder around 3.5 eV and a double peak between 4–5 eV instead of the two well defined experimental peaks at 3 and 5 eV. This double peak was also found in the calculation by Krasovska *et al.*[14] and the disagreement could be due to the experimental resolution. Furthermore, the experimental peak at 7.5 eV is confirmed by our results at about 7 eV. For the perpendicular component of the ϵ_2 spectrum [Fig. 4(b)], the peak around 3 eV arises from electronic transitions between the upmost occupied O 2p manifold and the unoccupied Ru t_{2g} bands. Due to the use of constant matrix elements in the joint density of states, the measured peak at 3 eV was not found in the LMTO-ASA calculations.[11] We also point out that the experimentally observed peak at 8.5 eV is somewhat shifted to lower energies in our calculation.

Figures 5 and 6 display a comparison between the calculated and experimental data for the parallel (a) and perpendicular (b) components of real and imaginary parts of the dielectric function for IrO_2, respectively.

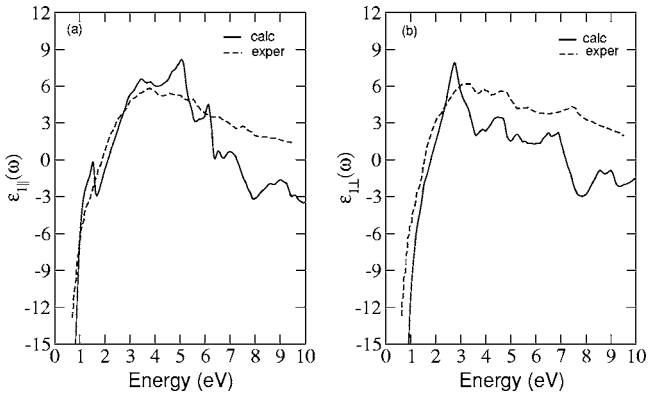

FIG. 5. Parallel (a) and perpendicular (b) components of the real part of the dielectric function versus photon energy for IrO_2.

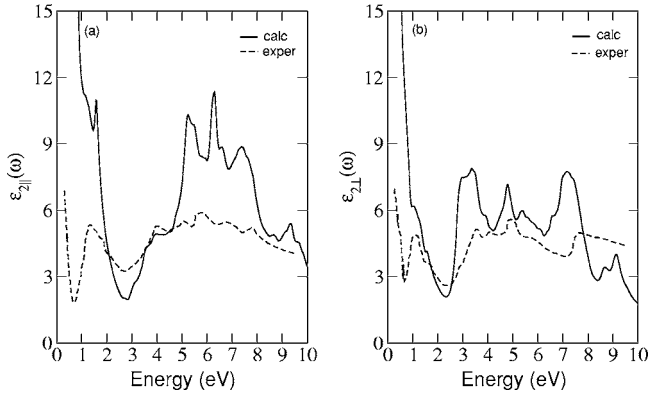

FIG. 6. Imaginary part of the dielectric function versus photon energy for IrO_2: parallel (a) and perpendicular (b) components.

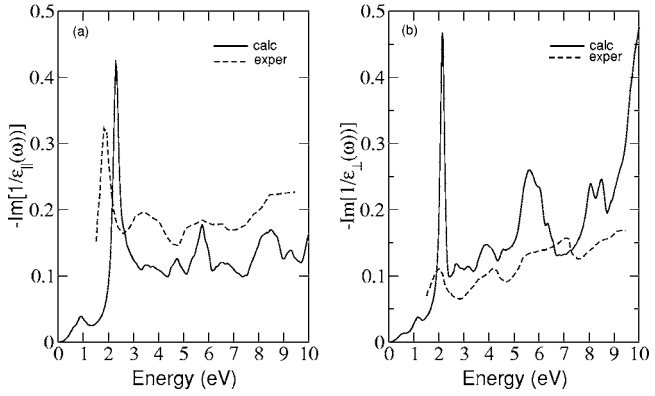

FIG. 7. Parallel (a) and perpendicular (b) components of the energy loss spectra as a function of photon energy for RuO_2.

At low energies, the intraband transitions play an important role and the large negative values of ϵ_1 [Fig. 5] for the parallel and perpendicular components indicating that the crystal has a Drude-like behavior whereas at higher energies the interband transitions take place giving rise to optical features. Similarly to RuO_2, from ϵ_2 spectra [Fig. 6] we see that IrO_2 has a high absorption for both polarizations at low energies. The peaks around 1.5 eV for both components of ϵ_2 spectra are assigned due to the intraband electronic transitions which occur within the Ir t_{2g} bands. Indeed, the width of the filled Ir t_{2g} bands is 2.6 eV and there are no $p \rightarrow d$ transitions allowed below this energy. The first peak due to $p \rightarrow d$ transitions occurs at 4 eV for the parallel component while its counterpart occurs at 3.1 eV for the perpendicular component. The second peak for the parallel component of ϵ_2 appears at 5.2 eV but its correspondent for the perpendicular component is somewhat smeared out and it appears as a shoulder around 4 eV. Additionally, the third peak appears at 6.3 and 4.8 eV for the parallel and perpendicular components, respectively. At energies around 7.4 eV the parallel component shows a peak which occurs at 7.2 eV for the perpendicular component.

The energy loss spectrum is calculated directly from the total dielectric function as

$$-Im\left[\frac{1}{\epsilon(\omega)}\right] = \frac{\epsilon_2(\omega)}{\epsilon_1(\omega)^2 + \epsilon_2(\omega)^2}. \quad (6)$$

In Fig. 7 we present the theoretical and experimental energy loss spectra for RuO_2: (a) parallel and (b) perpendicular components.

For a free-electron gas and in the absence of band to band transitions for the dielectric function, the plasma frequency occurs at the root of $\epsilon_1(\omega)$. However, when we consider intraband and interband electronic transitions the plasma frequency is shifted to higher energies and the root of $\epsilon_1(\omega)$ is now the threshold energy for the interband transitions. In the energy loss spectra, we see that both components show a peak at about 2 eV which are due to the roots of $\epsilon_1(\omega)$ and the features located at $\omega_p = 3.6$ eV and $\omega_p = 3.5$ eV, correspond to the parallel and perpendicular components of the plasma frequency, respectively. Our plasma frequencies show a good agreement with the theoretical values[14] of $\omega_p = 3.4$ and $\omega_p = 3.7$ eV for the parallel and perpendicular components whereas the experimental results for both polarizations are nearly 3.4 and 3.0 eV by Goel *et al.* and Modio *et al.*, respectively.[10,28]

The theoretical and experimental energy loss spectra for the parallel and perpendicular components for IrO_2 are shown in Figs. 8(a) and 8(b). As one can see, our energy loss spectrum shows a good agreement with the experimental data.[10] Optical transitions within the Ir $5d$ bands are responsible for the peaks at around 1.5 eV while our calculated plasma frequencies are $\omega_p = 3.1$ eV and $\omega_p = 4.2$ eV for the parallel and perpendicular components, respectively. As seen in Fig. 8, the experimental plasma frequencies for both polarizations are assigned as being the optical features at about 4 eV.

V. SUMMARY

We have studied electronic and optical properties of RuO_2 and IrO_2 using first principles calculations employing the full potential LAPW method. Our electronic structures show a small energy gap between oxygen $2p$ and metal d bands for RuO_2 whereas no p-d gap is found for IrO_2. Our results confirm the overestimated covalent character of these bands

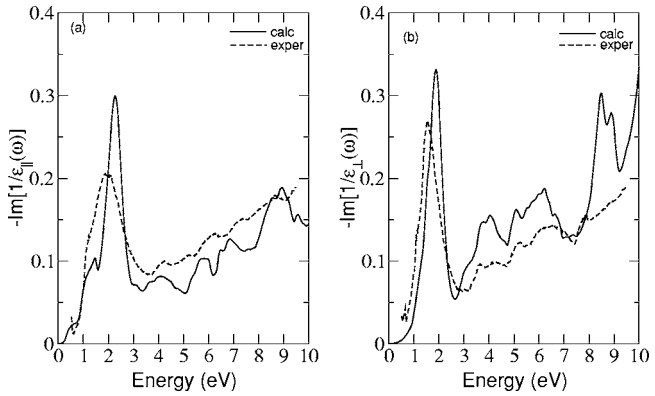

FIG. 8. Parallel (a) and perpendicular (b) components of the energy loss spectra, for IrO_2, as a function of photon energy.

found in earlier non-self-consistent calculations. Additionally, the electronic properties are in good agreement with experimental photoelectron data regarding the bandwidths and peak positions. By analyzing the optical properties, we find that these materials are good absorbers at low energies, where the dielectric functions show a Drude-like response. At higher energies, the optical features are assigned as electronic transitions arising from oxygen $2p$ to metal d bands. Our dielectric functions and energy loss spectra show a good agreement with optical measurements.

ACKNOWLEDGMENTS

This work was financially supported by the Brazilian National Research Council (CNPq), Swedish Research Council (VR), EU network (EXCITING), and STINT.

*Electronic address: jailton.almeida@fysik.uu.se

[1] D. Adler, Rev. Mod. Phys. **40**, 714 (1968).
[2] S. Trasatti, Electrochim. Acta **36**, 225 (1991).
[3] T. Kawai and T. Sakata, Chem. Phys. Lett. **77**, 87 (1980).
[4] M. V. Shafer and J. Armstrong, IBM Tech. Discl. Bull. **20**, 4633 (1978).
[5] J. D. Pedder, Science Technol. (USA) **2**, 259 (1976).
[6] Y. Igarashi, K. Tani, M. Kasai, K. Ashikaga, and T. Ito, Jpn. J. Appl. Phys., Part 1 **39**, 2083 (2000).
[7] S. Tankiewicz, B. Morten, M. Prudenziati, and L. J. Golonka, Sens. Actuators, A **95**, 39 (2001).
[8] S. Musić, S. Popović, M. Maljković, Ž. Skoko, K. Furić, and A. Gajović, Mater. Lett. **57**, 4509 (2003).
[9] L. F. Mattheiss, Phys. Rev. B **13**, 2433 (1976).
[10] A. K. Goel, G. Skorinko, and F. H. Pollak, Phys. Rev. B **24**, 7342 (1981).
[11] J. H. Xu, T. Jarlborg, and A. J. Freeman, Phys. Rev. B **40**, 7939 (1989).
[12] K. M. Glassford and J. R. Chelikowsky, Phys. Rev. B **47**, 1732 (1993).
[13] B. Yu. Yavorsky, O. V. Krasovska, E. E. Krosovskii, A. N. Yaresko, and V. N. Antonov, Physica B **225**, 243 (1996).
[14] O. V. Krasovska, E. E. Krasovskii, and V. N. Antonov, Phys. Rev. B **52**, 11825 (1995).
[15] K. M. Glassford and J. R. Chelikowsky, Phys. Rev. B **49**, 7107 (1994).
[16] P. I. Sorantin and K. Schwarz, Inorg. Chem. **31**, 567 (1992).
[17] P. Blaha, K. Schwarz, G. K. H. Madsen, D. Kvasnicka, and J. Luitz, WIEN2K, An Augmented Plane Wave+Local Orbitals Program for Calculating Crystal Properties (Karlheinz Schwarz, Technical, University Wien, Austria), 2001, ISBN 3-9501031-1-2.
[18] J. P. Desclaux, Comput. Phys. Commun. **1**, 216 (1969).
[19] D. D. Koelling and B. N. Harmon, J. Phys. C **10**, 3107 (1977).
[20] J. P. Perdew, K. Burke, and M. Ernzerhof, Phys. Rev. Lett. **77**, 3865 (1996).
[21] H. J. Monkhorst and J. D. Pack, Phys. Rev. B **13**, 5188 (1976).
[22] C. E. Boman, Acta Chem. Scand. (1947-1973) **24**, 116 (1970).
[23] C. L. McDaniel and S. J. Schneider, J. Res. Natl. Bur. Stand. **71**, 119 (1967).
[24] R. Kötz and S. Stucki, Electrochim. Acta **31**, 1311 (1986).
[25] J. Riga, C. Tenret-Noël, J. J. Pireaux, R. Caudano, J. J. Verbist, and Y. Gobillon, Phys. Scr. **16**, 351 (1977).
[26] P. A. Cox, J. B. Goodenough, P. J. Tavener, D. Telles, and R. G. Egdell, J. Solid State Chem. **62**, 360 (1986).
[27] C. Ambrosch-Draxl and J. O. Sofo (unpublished).
[28] G. Mondio, F. Neri, and M. Allegrini, J. Appl. Phys. **39**, 2083 (2000).